UCSF
UC San Francisco Previously Published Works

Title
Multiple sources of signal amplification within the B-cell Ras/MAPK pathway

Permalink
https://escholarship.org/uc/item/58v750sp

Journal
Molecular Biology of the Cell, 30(13)

ISSN
1059-1524

Authors
Mclaurin, Justin D
Weiner, Orion D

Publication Date
2019-06-15

DOI
10.1091/mbc.e18-09-0560

Peer reviewed

Multiple sources of signal amplification within the B-cell Ras/MAPK pathway

Justin D. Mclaurin and Orion D. Weiner*
Cardiovascular Research Institute and Department of Biochemistry and Biophysics, University of California, San Francisco, San Francisco, CA 94158

ABSTRACT The Ras-Map kinase (MAPK) cascade underlies functional decisions in a wide range of cell types and organisms. In B-cells, positive feedback-driven Ras activation is the proposed source of the digital (all or none) MAPK responses following antigen stimulation. However, an inability to measure endogenous Ras activity in living cells has hampered our ability to test this model directly. Here we leverage biosensors of endogenous Ras and ERK activity to revisit this question. We find that B-cell receptor (BCR) ligation drives switch-like Ras activation and that lower BCR signaling output is required for the maintenance versus the initiation of Ras activation. Surprisingly, digital ERK responses persist in the absence of positive feedback-mediated Ras activation, and digital ERK is observed at a threshold level of Ras activation. These data suggest an independent analogue-to-digital switch downstream of Ras activation and reveal that multiple sources of signal amplification exist within the Ras-ERK module of the BCR pathway.

INTRODUCTION

Digital or switch-like biochemical responses enable cells to convert gradual changes in external stimuli into binary cellular decisions such as differentiation and programmed cell death (Spencer and Sorger, 2011; Huang *et al.*, 2013). Positive feedback-driven protein activation is a common mechanism for generating digital signaling responses. Classic studies in *Xenopus* oocytes, for example, show how positive feedback within the Ras-Map kinase (MAPK) cascade results in digital activation of the terminal kinase, p42 MAPK (Ferrell and Machleder, 1998). Subsequent studies have implicated digital MAPK responses in coordinating processes ranging from yeast mating responses to *Drosophila* tracheal placode invagination (Malleshaiah *et al.*, 2010; Ogura *et al.*, 2018). Although the specific molecular details may vary across these organismal contexts, the

result is the same: each makes use of positive feedback impinging on the MAPK machinery to drive switch-like like activation of the terminal kinase (ERK in mammalian cells).

Cells of the B-cell lineage also exhibit digital ERK activation, but here this binary response is thought to be generated by positive feedback at the level of Ras activation rather than within the MAPK cascade (Das *et al.*, 2009). Here, the interplay of two Ras GEFs, Ras-GRP and SOS, form the basis of a positive feedback loop to generate switch-like activation of Ras. Following antigen receptor triggering, RasGRP generates a small amount of initiating RasGTP, which is then amplified via RasGTP-driven activation of SOS (Figure 1A) (Margarit *et al.*, 2003; Boykevisch *et al.*, 2006). Computational models of this minimal Ras-activating circuit posit a sharp transition (from off to on) in the Ras activation dose-response curve, characteristic of switch-like activation (Das *et al.*, 2009; Jun *et al.*, 2013; Iversen *et al.*, 2014). A potential result of this switch-like activation is a phenomenon known as hysteresis, a type of molecular memory in which Ras activity persists in the absence of continuous antigen receptor engagement (Das *et al.*, 2009). However, live Ras activation dynamics in these cells has never been directly observed.

Here we take a live-imaging approach to analyze Ras-ERK signaling in individual Ramos B-cells. We find that BCR engagement drives switch-like RasGTP responses at the single cell level, giving rise to bimodal Ras activation at the population level. Less receptor-based stimulation is required for the maintenance than for the initiation of a Ras response, providing evidence for hysteresis in Ras activation. Surprisingly we find that ERK responses remain binary
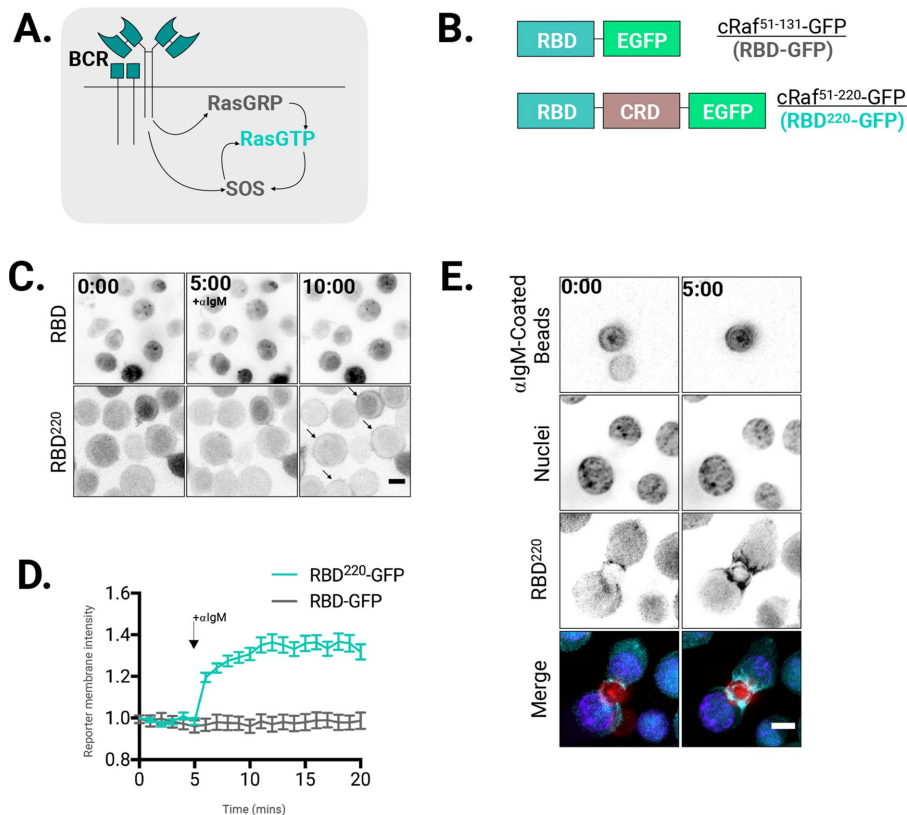

FIGURE 1: Visualizing Ras activation dynamics during B-cell activation in living cells. (A) Schematic of the Ras GEFs that drive Ras activation downstream of B-cell receptor triggering. (B) Domain structure of RasGTP biosensors. (C, D) Single cell image analysis of RasGTP biosensor localization following B-cell activation. (C) Representative images of RBD-GFP (top) and RBD^{220}-GFP (bottom) before and after addition of BCR agonist (αIgM, 10 μg/ml). Scale bar is 5 μm. Arrows highlight plasma membrane translocation of Ras biosensors, indicated by a halo of GFP signal around the cell periphery. (D) Quantitation of normalized Ras biosensor intensity on the plasma membrane. Arrow indicates time αIgM addition ($t = 5$ min). Data are means of $n = 40$ single cell traces. Traces were generated by first inverting single cytosolic RBD^{220}-GFP traces (to approximate membrane intensity), then normalizing individual traces to prestimulus mean, and last, averaging single traces to generate a single curve. This method was used here and in all subsequent figures. See *Materials and Methods* for details on data collection and quantitation. (E) Representative images of RBD^{220}-GFP localization in cells initially contacting BCR agonist αIgM-coated beads at the moment of contact (first column) and 5 min after contact (second column). Scale bar 5 μm.

even in the absence of positive feedback-driven Ras activation. This work supports multiple analogue-to-digital switches in B-cell activation, both at the level of Ras activation and between Ras activation and ERK activation.

RESULTS

Visualizing Ras activity during B-cell activation

Several groups have leveraged the high-affinity (~20 nM) interaction between the Raf-1 Ras-binding domain (Raf1$^{51-131}$, known as RBD) and RasGTP to generate FRET and membrane translocation-based reporters to quantify Ras activity in living cells (Mochizuki *et al.*, 2001; Chiu *et al.*, 2002; Oliveira and Yasuda, 2013). However, these approaches often lack the sensitivity to detect endogenous Ras and require overexpression of Ras proteins to produce a detectable signal, potentially altering Ras regulation. Alternatively, endogenous RasGTP has been detected in live cells using a reporter in which RBD is multimerized (to increase avidity) and mutagenized (to decrease affinity), but this approach has the potential difficulty of

responding to Ras density or sequestering endogenous Ras due to the high avidity of the multimeric reporter (Augsten *et al.*, 2006; Rubio *et al.* 2010). To circumvent these issues, we make use of an extended fragment of cRaf/Raf1 that includes a second Ras-binding site, the cysteine-rich domain (Williams *et al.*, 2000; Thapar *et al.*, 2004). This monovalent probe, Raf1$^{51-220}$ (which we refer to as RBD^{220}), was previously shown to detect endogenous levels of Ras-GTP in a variety of cell types with 1:1 stoichiometry (Bondeva *et al.*, 2002; Hibino *et al.*, 2009; Anderson *et al.* 2011). When expressed in Ramos B-cells, RBD^{220} tagged with eGFP (RBD^{220}-GFP) rapidly translocated to the plasma membrane as indicated by a halo of GFP signal around the periphery of the cell following stimulation with BCR cross-linking F(ab')$_2$ fragments (αIgM) (Figure 1, B and C; Supplemental Movie 1). RBD-GFP, by contrast, failed to translocate to the membrane on αIgM stimulation (Figure 1, B and C). We adapted an analysis pipeline to quantitate RBD^{220} membrane association by quantifying Ras reporter cytoplasmic depletion and approximating reporter membrane enrichment as the inverse of this signal (Takeda *et al.*, 2012). Using this method, we observed an ~37% increase in RBD^{220} on the membrane following BCR cross-linking with saturating amounts (10 μg/ml) of αIgM (Figure 1D; Supplemental Figure S1, A–C). GFP-tagged RBD, by contrast, showed no discernable membrane translocation or measurable cytoplasmic depletion to the same stimulus.

Previous work in which RBD^{220} was transfected into adherent cell lines suggested that this probe could inducibly, but possibly, irreversibly associate with active Ras molecules on the membrane, thereby impairing downstream ERK activation (Bondeva *et al.*, 2002). In contrast, for Ramos B-cells stably expressing this probe, we find that RBD^{220} membrane association is responsive to both the initiation and (as we will show in subsequent figures), the termination BCR signaling (Figure 1D). Furthermore, flow cytometry analysis of RBD^{220}-expressing cells showed no alteration in the levels or kinetics of ERK phosphorylation (ppERK) compared with control cells, indicating that this Ras reporter does not perturb downstream signaling (Supplemental Figure S2) for the level of reporter expression used in our experiments. Pretreating Ramos cells with Syk (BAY-61-3606) inhibitor abolished αIgM-induced RBD^{220} translocation to the membrane, whereas stimulating cells with the activator protein kinase C (PKC)/RasGRP agonist, phorbol 12,13-dibutyrate (PDBu) drove rapid reporter translocation (Supplemental Figure S3A). Pulsing untreated RBD^{220} reporter cells with Syk inhibitor drove a rapid decline (~50% on average) in Ras reporter membrane association (Supplemental Figure S3B), indicating the extent of tonic signaling in nonstimulated cells. When RBD^{220} reporter cells were incubated with αIgM-coated beads, RBD^{220} localized to the region of contact between the cells and beads,

reminiscent of an immunological synapse (Figure 1E; Supplemental Movie 2). Together, these data indicate that RBD[220] can be used as a sensitive dynamic reporter of BCR-stimulated Ras activation.

Analogue Ras activation driven by PKC/RasGRP

In B-cells, Phospholipase Cγ2 is recruited to the membrane following BCR ligation, where it catalyzes the cleavage of PI(4,5)P2 into diacylglycerol (DAG) and Inositol trisphosphate (Supplemental Figure S4A). This DAG recruits and activates RasGRP and its activator PKC to initiate RasGTP production. Transfection studies performed with full-length RasGRP1 showed that overexpression of this protein produces linear increases in expression of the distal Ras-ERK signaling effector CD69 as a function of RasGRP1 expression level (Das *et al.*, 2009). Similar experiments performed with the catalytic domain of SOS (SOS_cat) showed that this protein induced exponen-

tial increases of CD69 expression as a function of SOS_cat expression level (Das *et al.*, 2009). Whereas these and other experiments suggest that RasGRP proteins drive analogue increases in RasGTP, the expression dynamics of distal Ras-ERK effectors can serve as poor indicators for upstream Ras signaling dynamics (Wilson *et al.*, 2017). Moreover, the activity of RasGRP proteins is subject to complex regulation by DAG, Ca^{2+} levels, and phosphorylation, making it difficult to infer how RasGTP responses are regulated by RasGRP activity alone (Teixeira *et al.*, 2003; Zheng *et al.*, 2005; Iwig *et al.*, 2013).

To probe how Ras activation responds in the absence of SOS-driven feedback, we performed dose-response experiments with PDBu, a chemical mimetic of DAG. PDBu binds and recruits the Ras GEF RasGRP to the membrane but does not recruit or activate SOS (Lorenzo *et al.*, 2000). Western blot analysis revealed titratable induction of RasGRP3 T133 phosphorylation (a PKC phosphorylation site) on PDBu addition, validating this approach as a means of titrating RasGRP activity (Supplemental Figure S5A). Importantly, PDBu stimulation did not induce an increase in global phosphotyrosine or the recruitment of GRB2 to the membrane, both of which are prerequisites for SOS membrane recruitment and activation (Supplemental Figures S4, B and C, and S5A). Moreover, pretreating cells with the PKC inhibitor Gö6983 abolished PDBu-driven RBD[220] membrane recruitment and ppERK, confirming the necessity of this enzyme in sustaining PDBu-driven RasGTP levels (Supplemental Figure S4C).

To analyze how Ras signaling changes as a function of RasGRP activity at the single cell level, we stimulated RBD[220] reporter Ramos cells with different concentrations of PDBu and quantified RBD[220] cytoplasmic depletion via time-lapse microscopy. These dose-response experiments showed an acute increase in RBD[220] membrane recruitment that varied in mean amplitude as a function of PDBu dose (Figure 2, B and C). While similar fractions of cells responded to all doses of PDBu (ranging from 83% at 0.01 μM to 96% at 10 μM) (Supplemental Figure S5B), at the population level we observed a gradual increase in the distribution of mean RBD[220] membrane intensity as the PDBu concentration increased (Figure 2D). Consistent with this, we found that all doses of PDBu drove unimodal increases in RBD[220] membrane intensity (Figure 2D) as assessed by Hartigans' dip test, a statistical test that distinguishes between bimodal and unimodal population distributions that has been previously used to distinguish between bimodal and unimodal signaling responses (Hartigan and Hartigan, 1985; Das *et al.*, 2009; Jun *et al.*, 2013). Fitting these data with a Hill function produced an estimated Hill coefficient (nH) of 0.5 (Figure 2E). These data suggest that PKC/RasGRP drive analogue (nonultrasensitive) RasGTP production when triggered in the absence of SOS, consistent with previous reports (Das *et al.*, 2009).
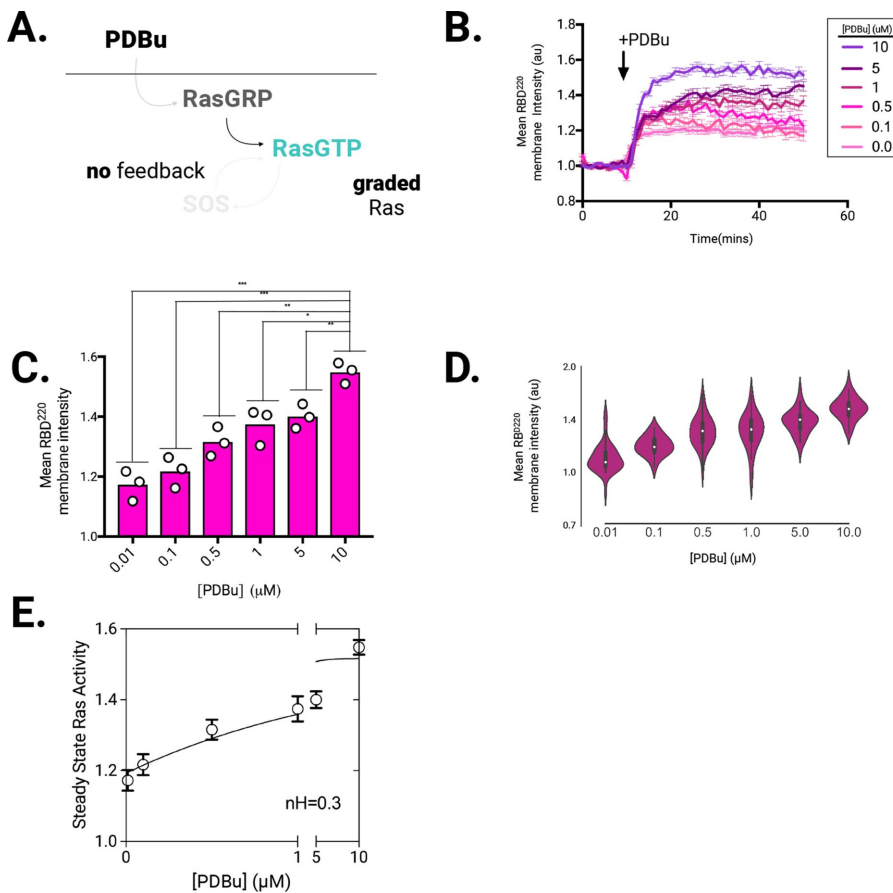

FIGURE 2: A water-soluble DAG mimetic (PDBu) drives graded, unimodal Ras activation responses. (A) Schematic of dose-response experiment for cells exposed to step function increases of PDBu (RasGRP agonist) of different amplitudes. PDBu recruits RasGRP to the membrane and unlocks its catalytic activity. (B–E) Live cell analysis of RBD[220]-GFP membrane association (henceforth referred to as Ras activation) in response to PDBu. (B) Dose response. Median intensity traces of cells stimulated with indicated doses of PDBu (see inset) over time. Arrow indicates time of PDBu addition (at ~t = 10 min). Error bars are SEM. Median intensity traces are generated from at least 50 cells per PDBu dose. Traces are representative of three independent experiments. (C) Mean RBD[220] membrane intensity (calculated from t = 20–40 min) from cells stimulated as indicated in B. Each circle represents the mean response from an individual experiment (n = 3). *$p < 0.05$, **$p < 0.01$, ***$p < 0.001$; ns (not significant) are used to denote statistical significance (two-tailed unpaired Student's t test). (D) Violin plots of cells stimulated as indicated in B showing unimodal Ras activation responses at all PDBu doses. Mean response to indicated dose of PDBu (*x*-axis) was calculated as the mean membrane intensity on a per-cell basis between t = 20–40 min (n = 50 cells displayed per PDBu dose). (E) Steady-state Ras activity (see *Materials and Methods*) across PDBu dose-response experiments. nH (inset) indicates Hill coefficient, showing lack of Ras ultrasensitivity for PDBu input.
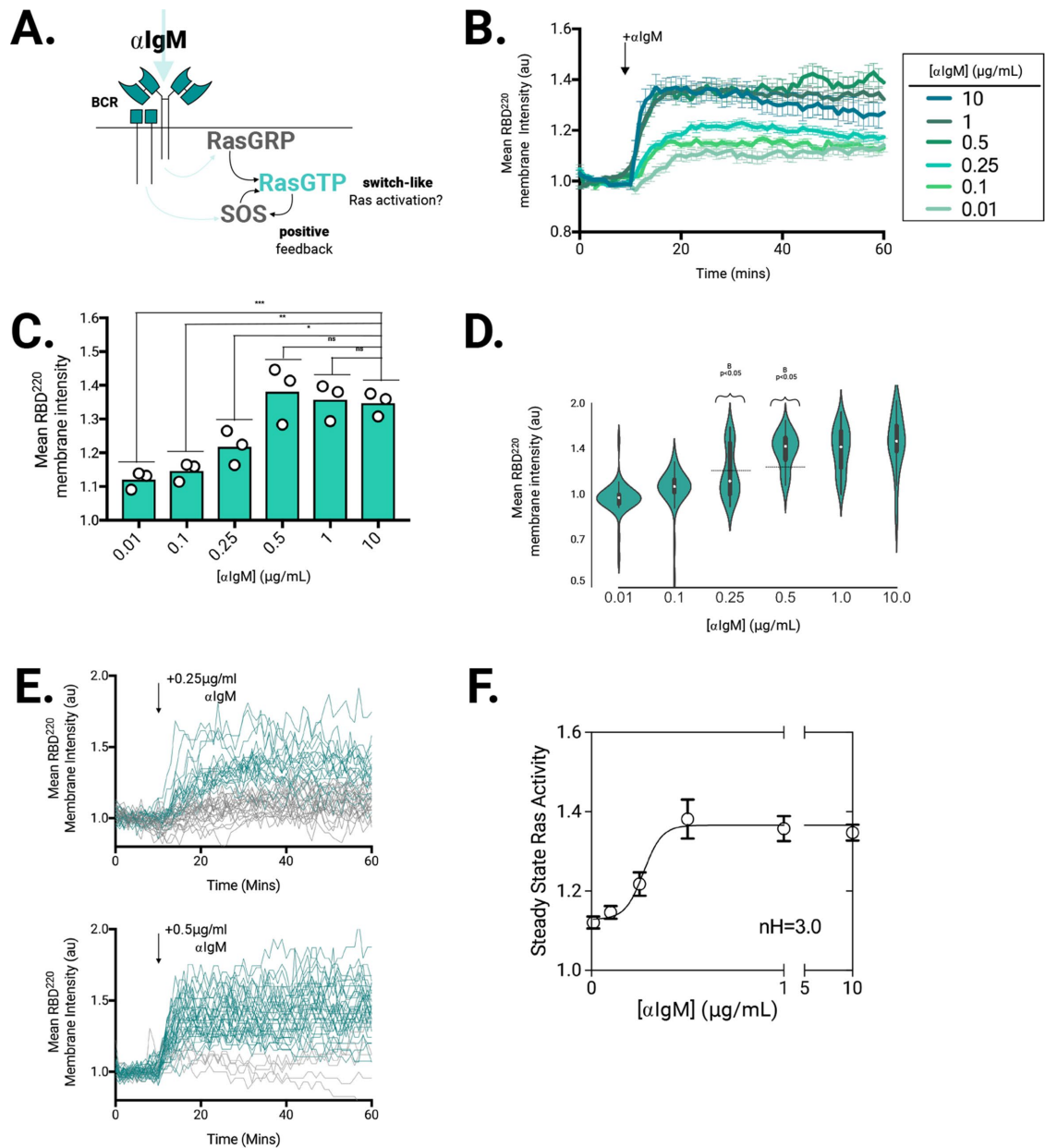
FIGURE 3: BCR agonist drives switch-like, bimodal Ras activation. (A) Schematic of dose-response experiment for cells exposed to step increases of BCR agonist (αIgM) of different amplitudes. (B–E) Live cell analysis of RBD^{220}-GFP membrane association. (B) Mean intensity traces of cells stimulated with indicated doses of αIgM (see inset) over time. Arrow indicates time of αIgM addition (at ~t = 10 min). Error bars are SEM. Mean intensity traces are generated from at least 50 cells per αIgM dose. Traces are representative of three independent experiments. (C) Mean RBD^{220} membrane intensity (t = 20–40 min) from cells stimulated as indicated in B. Each circle represents the mean response from an individual experiment (n = 3). *p < 0.05, **p < 0.01, ***p < 0.001, ns (not significant) are used to denote statistical significance (two-tailed unpaired *Student's t test*). (D) Violin plots of cells stimulated as indicated in B showing bimodal Ras activation at intermediate doses of αIgM. Steady-state response to indicated dose of αIgM (*x*-axis) calculated as the mean membrane intensity between t = 20–40 min (n = 50 cells displayed per αIgM dose). Bimodality (B) and p values were computed by Hartigans' dip test (see *Materials and Methods*). Dashed line indicates the dip statistic of cells stimulated with 0.25 and 0.5 μg/ml αIgM (see *Materials and Methods*). (E) Representative single cell traces (n = 40 cells per panel) from cells stimulated with 0.25 μg/ml (top) and 0.5 μg/ml (bottom) αIgM. Traces from responding cells are colored in teal, whereas nonresponding cells are colored gray. (F) Steady-state Ras activity (see *Materials and Methods*) across αIgM dose-response experiments. nH (inset) indicates Hill coefficient, demonstrating ultrasensitive Ras response for BCR agonist.

Switch-like induction in BCR-driven Ras responses

We next analyzed RasGTP signaling dynamics in the context of full BCR signaling. BCR ligation activates both RasGRP and SOS, and we reasoned that titrating BCR output could serve as a means of tuning the activity of these proteins. The αIgM stimulation drove dose-dependent increases in global phosphotyrosine production, validating our ability to titrate receptor output with this approach (Figure 3A; Supplemental Figure S5A). Low-level (0.25 μg/ml and
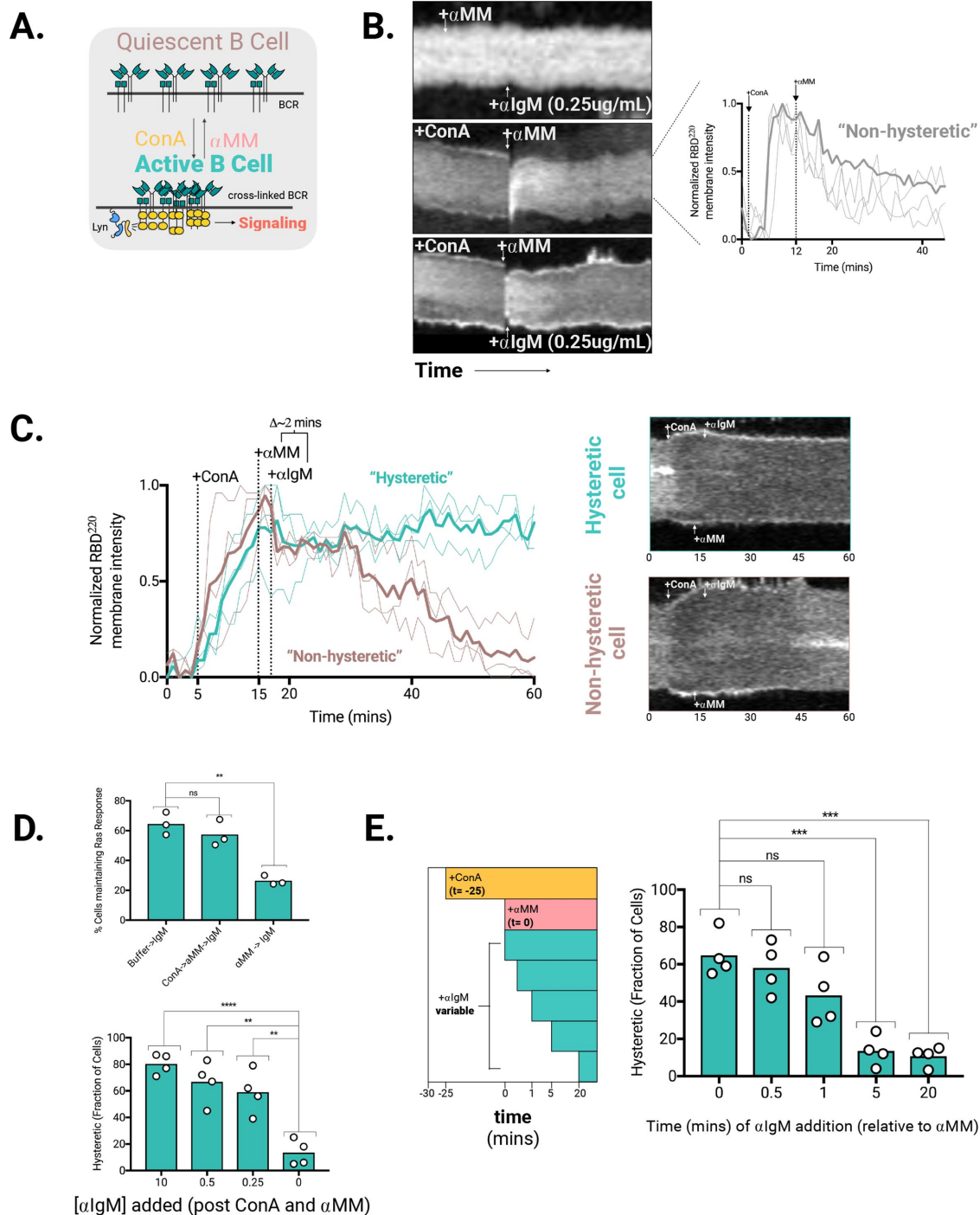
FIGURE 4: Hysteresis in BCR-driven Ras activity. (A) Schematic of the reversible BCR triggering assay relying on ConA-mediated receptor cross-linking, and αMM-mediated reversal of B-cell receptor cross-linking. Lyn (a Src-family kinase) phosphorylates cross-linked receptors, leading to downstream signaling. (B) Single cell kymographs of RBD[220]-GFP over time. (Top) Cells stimulated with 100 mM αMM (at $t = 2$ min), followed by 0.25 μg/ml αIgM (at $t = 12$ min). (Middle, left) Cells stimulated with 50 μg/ml ConA ($t = 2$ min) followed by 100 mM αMM ($t = 12$ min). (Middle, right) Single cell traces from representative nonhysteretic cells showing rapid ConA-induced Ras responses that are attenuated on the addition of αMM. (Bottom) Cell stimulated with 50 μg/ml ConA (at $t = 2$ min), 100 mM αMM ($t = 12$ min), and 0.25 μg/ml αIgM (at $t = 13$ min). Experiment run length is 45 min. (C) (Left) Single cell traces showing examples of cells responding in a hysteretic (turquoise) or "nonhysteretic" (brown) manner following stimulation with 50 μg/ml ConA (at $t = 5$ min), 100 mM αMM ($t = 15$ min), and 0.25 μg/ml αIgM (at $t = 17$ min). (Right) Example kymographs of a hysteretic (top, turquoise border) and nonhysteretic (bottom, brown border) are displayed. (D) (Top) Comparison of the effect of ConA and/or αMM pretreatment on the fraction of cells responding to 0.25 μg/m αIgM. RBD[220]-GFP expressing Ramos cells were pretreated with either imaging media (buffer, right column), 50 μg/ml ConA (for 5 min), and then 100 mM αMM (for 2 min) (center column) or 100 mM αMM (for 20 min) (right column) prior to stimulation with 0.25 μg/ml αIgM. (Bottom) The fraction of hysteretic cells stimulated as in C in which the concentration of αIgM is

below) stimulation with BCR agonist elicited dose-dependent increases in the rate and mean amplitude of Ras activity, whereas high-level (0.5 µg/ml and above) stimulation yielded saturating response rates and amplitudes (Figure 3, B and C). In addition, Ras responses were, on average, persistent (>50 min) at all αIgM doses applied.

At the population level, the fraction of cells responding to αIgM stimulation ranged from 35% at 0.0 1 µg/ml to 92% at 10 µg/ml, increasing as a function of αIgM dose (Supplemental Figure S5D). Hartigans' dip test analysis level showed unimodal steady-state Ras responses at the two lowest (0.01 and 0.1 µg/ml) and highest (1 and 10 µg/ml) doses of αIgM stimulation but bimodal distributions at intermediate doses (0.25 and 0.5 µg/ml, $p < 0.05$, respectively) (Figure 3D). Indeed, we observed that single cell traces from cells stimulated with 0.25 and 0.5 µg/ml show a similar bifurcation in response following αIgM stimulus, with some cells responding robustly and other cells showing weak or no response (Figure 3E). Consistent with these observations, steady-state Ras responses showed a sharp transition with an estimated nH of 3, consistent with switch-like activation of Ras following BCR triggering (Figure 3F).

Hysteresis in BCR-driven Ras activation

SOS-driven positive feedback is predicted to transiently maintain RasGTP levels (i.e., hysteresis) in cells in which signal flux through the BCR pathway is halted via antigen removal (Chakraborty et al., 2009; Das et al., 2009). This hysteresis in Ras activity is presumably mitigated via stable association of SOS with the plasma membrane, as has been observed in several cell types (Christensen et al., 2016).

To date, most efforts have leveraged ensemble biochemical and fixed-cell readouts to analyze hysteresis in RasGTP responses downstream of the BCR. Although these approaches have powerfully demonstrated B-cell's ability to maintain high levels of RasGTP in the absence of persistent receptor triggering, several lingering questions warrant a reassessment of this model via the analysis of individual living cells. 1) Does maintenance of Ras activity depend on the relative timing with which cells experience BCR receptor triggering? 2) How heterogenous are hysteretic Ras responses across a population of cells? We paired our live imaging set up with a previously developed means for reversibly controlling antigen receptor triggering to answer these questions (Weiss et al., 1987). The lectin concanavalin A (ConA) binds and cross-links the BCR and has been previously used as a surrogate BCR ligand. BCR cross-linking by ConA can be rapidly attenuated via the addition of the high-affinity ConA-binder methyl α-D-mannopyranoside (αMM), providing a means to induce and revert BCR signaling (Figure 4A). Indeed, we find that ConA rapidly induces RBD^{220} membrane association, and the addition of αMM terminates Ras activation (Figure 4B, middle left and right panels). Importantly, BCR surface expression is required for ConA-induced signaling, as ConA does not drive RBD^{220} membrane association in immunoglobulin M (IgM)-deficient cells despite retaining its ability to associate with the cell surface (Supplemental Figure S6B). These experiments validate ConA/αMM system as a reversible receptor triggering system compatible with our live imaging system.

Hysteresis in Ras activation predicts that less receptor signaling is required to maintain Ras activity than to initiate it in the first place (Das et al., 2009). We aimed to use the ConA/αMM system to test this directly. We found that in cells pretreated with 100 mM αMM that even saturating doses of αIgM (10 µg/ml) exhibited attenuated signaling responses, possibly due to osmolarity differences in the media of αMM-pretreated cells (Supplemental Figure S7A). Dose-response experiments revealed that 0.25 µg/ml αIgM was the minimum stimulus required to induce a Ras response in cells pretreated with αMM (Supplemental Figure S7B). We therefore used 0.25 µg/ml αIgM as the minimal BCR-ligand dose for experiments aimed at examining hysteresis in Ras signaling in these cells.

We cross-linked surface BCR with a high dose of ConA (50 µg/ml), relieved those cross-links with αMM (100 mM), and recross-linked receptors with a low dose of αIgM (0.25 µg/ml) while monitoring RBD^{220} translocation dynamics. Ras activity was maintained in 59% of cells in response to the iterative addition of ConA, αMM, and αIgM (Figure 4, B–E). We termed these cells "hysteretic" and defined them as those whose Ras activity returns to within the 80th percentile of their maximum post-ConA level following the ConA/αMM/αIgM stimulus regimen (Figure 4C). ConA/αMM-treated cells restimulated with either saturating (10 µg/ml) or minimal (0.25 µg/ml) αIgM stimulus displayed higher (and statistically significant) fractions of hysteric cells than cells treated with control media (Figure 5D), suggesting a requirement for reengaging the BCR to maintain a Ras response in this scenario. Interestingly, we found that the delay between primary stimulus termination (αMM addition) and minimal stimulus application (αIgM) played a significant role in determining the fraction of hysteretic cells. Statistically similar but nevertheless declining fractions of hysteretic cells were found in instances where αIgM was added within ~1 min of αMM addition (Figure 4E). In contrast, the addition of αIgM at 5 and 20 min post-αMM addition drove a statistically significant decrease in the fraction of hysteretic cells (Figure 4E), suggesting a temporal window in which Ras activity may be maintained before committing to decay.

Signal amplification downstream of Ras

How are switch-like Ras signals decoded by the downstream MAPK machinery (Figure 5A)? SOS-mediated feedback is thought to drive the bimodal pattern of ppERK seen in active lymphocytes (Das et al., 2009). Consistent with this, we found that Ramos B-cells exhibit a bimodal pattern of ppERK following BCR cross-linking with αIgM (Figure 5B, left). To test whether this binarization of ERK responses originates at the level of Ras activation, we supplemented our cell line coexpressing RBD^{220} with the recently described live cell ERK kinase translocation reporter (ERK-KTR) (Regot et al., 2014). Thus, coexpression of these reporters in the same cell allowed us to correlate Ras and ERK activity with high temporal precision in the same individual living cell (Figure 5C; Supplemental Movie 3).

In ensemble average responses, we found that low doses of αIgM (0.01 and 0.1 µg/ml) failed to increase ERK kinase activity (as read-out by ERK-KTR signal) despite driving detectable increases in RBD$^{220.}$ membrane association (Figure 5D). Interestingly, these low

varied. Each circle represents a single experiment. At least 20 cells were quantified per experiment. ***$p < 0.001$ and **$p < 0.01$ denote statistical significance (two tailed unpaired Student's t test). (E) (Left) Schematic depicts the timing of of ConA (at $t = -25$ min) and αIgM (variable time points) addition relative to the time of αMM addition ($t = 0$ min). (Right) Quantitation of the fraction of hysteretic cells as a function of time of αIgM addition relative to αMM addition. Hysteretic cells are defined as those whose Ras activity returns to within the 80th percentile of their maximum post-ConA level following the addition of αIgM. Each circle represents a single experiment. At least 20 cells were quantified per experiment. ***Statistical significance ($p < 0.001$, two-tailed unpaired Student's t test).
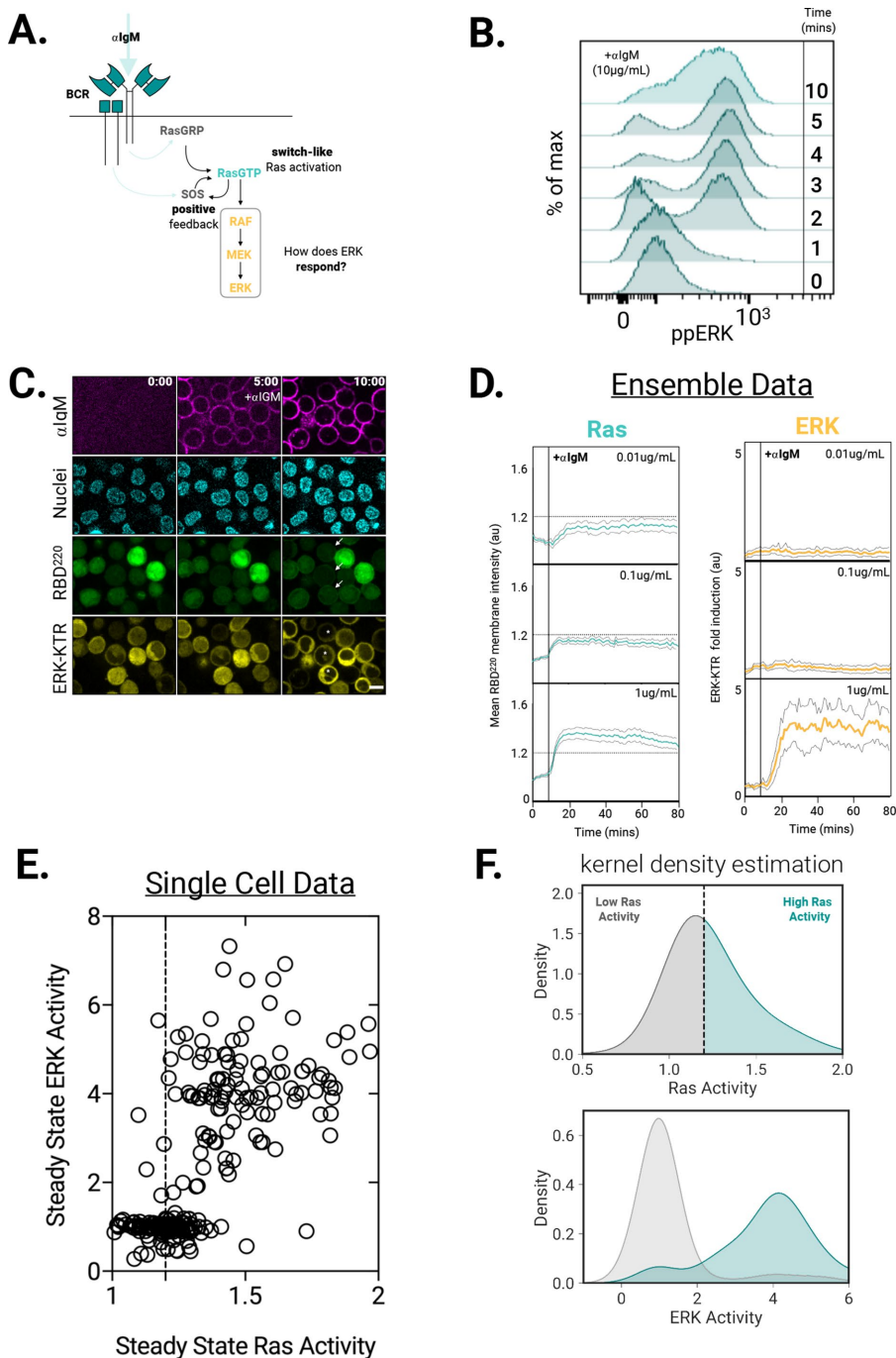
A.

B.

C.

D. Ensemble Data

E. Single Cell Data

F. kernel density estimation

FIGURE 5: Bimodal ERK activation beyond a threshold level of Ras activation. (A) Schematic depicting switch-like Ras activation arising from BCR-generated Ras positive feedback. (B) ppERK time course from wild-type Ramos B-cells stimulated with αIgM (10 µg/ml, right) (representative of three independent experiments). (C) Representative ($n = 2$) time course images of αIgM (top, magenta), nuclei (second row, teal), RBD[220]-GFP (third row, green), and ERK-KTR-TagRFP-T (yellow, bottom) following APC-αIgM addition (10 µg/ml). Nuclei are labeled with NucBlue (see *Materials and Methods*); 5 µm scale bar. (D) Cells coexpressing RBD[220]-GFP (left, purple) and ERK-KTR-TagRFP-T (right, brown) were stimulated with indicated doses (inset) of αIgM. Mean response (50 cells per trace; pooled from three independent experiments) plotted over time. The 95% confidence interval (black lines) envelope mean traces. Dashed lines (left column) indicate apparent threshold of Ras activity required to trigger ERK response (~20% increase above basal). (E) Dose-response experiments. Representative single cell mean steady-state ERK activity plotted as a function of mean steady-state Ras activity in individual cells. Each circle is data from an individual cell. Data are pooled from αIgM dose-response experiments where cells were stimulated with 0.01, 0.1, 0.25, 1, or 10 µg/ml αIgM. Fifty cells per αIgM dose are plotted (250 cells total). Dashed line indicates

doses of αIgM stimulus generally drove a <20% increase in RBD[220] membrane association, suggesting that a threshold increase in Ras activity above basal levels may be required to trigger an ERK response in these cells. Ensemble averages of cells stimulated with a higher dose (1 µg/ml) of αIgM, by contrast, drove a >20% increase in RBD[220.] membrane association and also induced potent ERK-KTR responses (Figure 5D, bottom right). We therefore hypothesized that a 20% increase in Ras activity may be required for inducing an ERK response in αIgM-stimulated cells.

To test this hypothesis, we analyzed Ras (RBD[220]-GFP membrane association) and ERK (ERK-KTR activity) in individual cells stimulated with αIgM concentrations spanning three orders magnitude (Figure 5E). To compare responses across stimulus doses, we plotted single cell Ras and ERK activity at steady state (that is once signaling responses have stabilized following αIgM addition). We observed a sharp increase in ERK activity in cells whose Ras activity exceeded a 20% increase above basal levels (Figure 5E), which is notably the same threshold that separates the two bimodal populations of Ras activation seen following anti-IgM (Figure 3D). By contrast, very few cells with <20% increase in steady-state Ras activity showed detectable increases in steady-state ERK activity (Figure 5E). Interestingly, we observed that many cells with large (>20%) increases in Ras activity showed no detectable changes in ERK, indicating that surpassing this Ras threshold does not ensure ERK activation but may represent the threshold of ERK bistability. We therefore sought to understand the population level distribution of ERK responses as a function of Ras activity. Kernel density estimation (bandwidth = 0.5) of these data showed that >20% increases in Ras activity corresponded > four-fold increase in median ERK kinase activity, with the population density exhibiting a bimodal transition (Figure 5F).

Bimodal responses are generated by switch-like systems responding in an all-or-none manner to stimuli above a threshold while ignoring subthreshold stimuli (Ferrell and Ha, 2014). While our analysis would be consistent with switch-like activation of Ras

---

20% increase above basal Ras activity. (F) Kernel density estimations of Ras and ERK activity plotted in E. Ras activity (top) is segmented into low and high by line (vertical, dashed line) demarcating a 20% increase above basal activity. ERK activity (bottom) is plotted as a function of low (gray) and high (teal) Ras activity.
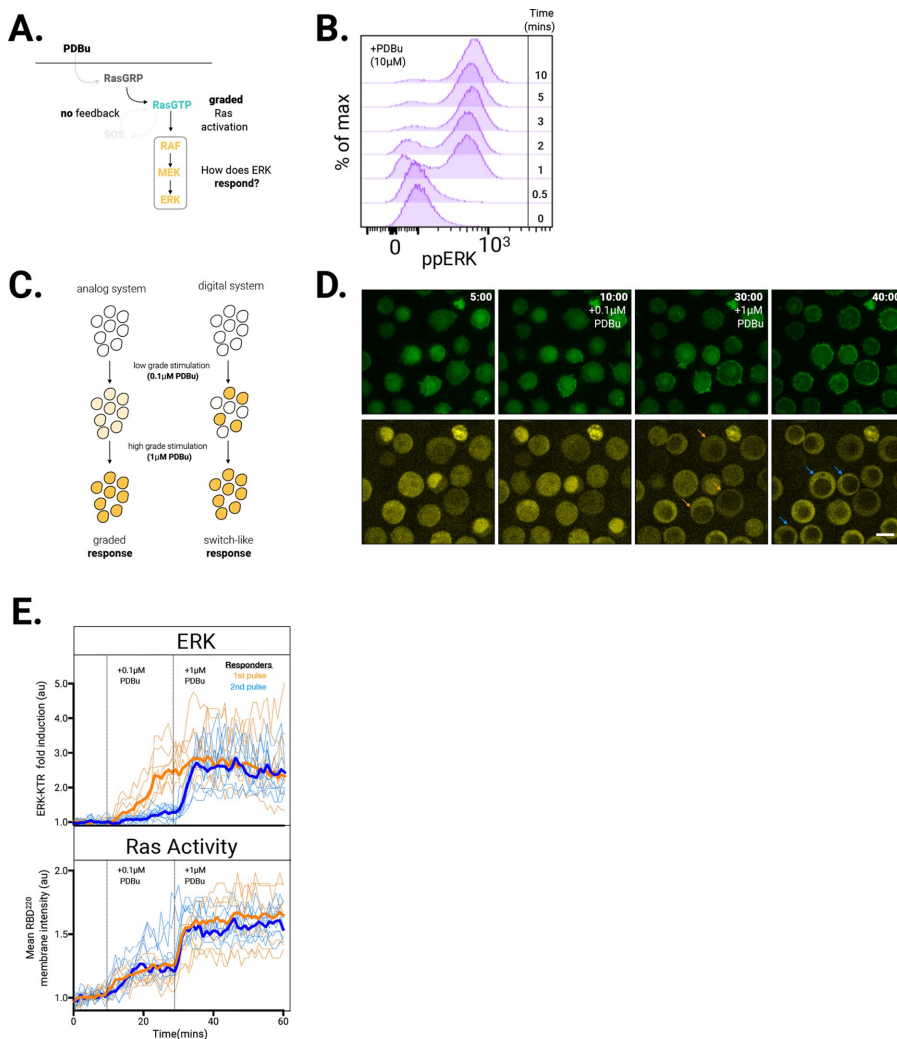
FIGURE 6: Digital ERK activation downstream of Ras. (A) Schematic depicting graded Ras activation driven by PDBu-mediated activation of RasGRP (this agonist does not engage the Ras positive feedback loop). (B) ppERK time course from wild-type Ramos B-cells stimulated PDBu (10 μM, right) (representative of three independent experiments). (C) Possible outcomes of an experiment in which analogue (left) and digital (right) cellular systems are pulsed sequentially with low and high doses of PDBu. Graded increases are characterized by gradual increases in cell responses (left, yellow coloration). Switch-like responses are characterized by all-or-none responses on a per-cell basis (right, yellow coloration). (D) Representative ($n = 3$) time course images of RBD^{220}-eGFP and ERK-KTR-TagRFP-T Ramos cells stimulated with 0.1 μM (at $t = 10$ min) and 1 μM PDBu (at $t = 30$ min). Arrows indicate ERK-KTR expressing cells responding to the first (orange) or second (blue) pulse of PDBu. (E) Single cell traces of cells stimulated as in D depicting Ras (top) and ERK (bottom) responses. Traces are color coded to indicate cells whose ERK-KTR responses initiated at the first (orange) or second (blue) pulse of PDBu.

simply propagated to ERK without further amplification, it is formally possible that bimodal ERK responses are generated downstream of Ras via independent feedback modules (Ferrell and Machleder, 1998; Shindo *et al.*, 2016). To test this idea, we stimulated cells with PDBu (a condition in which Ras positive feedback is not engaged and for which Ras activation is graded, not bimodal) and analyzed the resulting ERK responses in single cells (Figure 6A). Surprisingly, we found that in PDBu-stimulated Ramos cells, bimodal ppERK is retained and is kinetically similar to BCR-activated cells (Figures 6B and 5B). Importantly, we found that this bimodal activation is preserved across a wide range of PDBu doses in both Ramos and Jurkat T-cells, suggesting conservation of the underlying signaling network architecture leading to bimodal ERK downstream of unimodal Ras

(Supplemental Figure S8, A, right panel, and B). This led us to hypothesize that ERK may respond in a digital manner to changes in Ras activity. To test this, we performed two-step experiments in which we pulsed cells sequentially with low (0.1 μM) and high (1 μM) doses of PDBu, reasoning that analogue increases in Ras activity driven by PDBu would allow for analysis of ERK responses in the absence of upstream feedback (Figure 6C). Live imaging of RBD^{220} showed two step-like increases of plasma membrane translocation in response to sequential pulses of low and high PDBu stimulus, consistent with analogue Ras activation (Figure 6, D and E, bottom). In contrast (for the same cells), ERK-KTR responded to either low or high pulses of PDBu, with each cell exhibiting a single step-like response despite experiencing two pulses of stimuli (Figure 6, D and E, top). Taken together, these data suggest that an increase in Ras activity above a threshold is necessary to trigger downstream ERK signaling. Furthermore, the Ras/MAPK cascade contains two independent modules for generating bimodal responses—one within and one downstream of Ras activation.

DISCUSSION

In this work we provide evidence for multiple signal amplification steps occurring at the level of Ras and ERK during B-cell activation. BCR-driven Ras activation is highly switch-like (nH = 3), whereas PDBu-driven Ras activation is graded (nH = 0.3), supporting the model that cooperation between RasGRP and SOS gives rise to nonlinear bimodal Ras pathway activation (Das *et al.*, 2009) (Figures 2E and 3F). Less receptor-based stimulation is required to maintain a Ras response than to initiate it, consistent with hysteresis in BCR-Ras-GTP dose-response curve (Figure 3C; Das *et al.*, 2009). ERK activation is bimodal in BCR-triggered Ramos cells, and these bimodal responses proceed following Ras activation beyond a strict threshold (Figure 5, B and E) that also corresponds to the threshold that separates the two bimodal populations of Ras. Surprisingly, ERK regulation is digital in its own right, exhibiting all-or-none activation even for inputs that fail to generate digital Ras responses (Figure 6, B and E). Although these findings broadly support the predominant model for digital Ras activation in active lymphocytes, they also deviate from this model in several key ways, raising important questions concerning the mechanistic basis for digitization of ERK signaling.

Previous studies have leveraged SOS mutant transformed DT40 B-cell lines, Jurkat T-cells and primary mouse T-cells along with population-based fluorescence activated cell sorting (FACS) measurements of ppERK, to conclude that SOS is required for digital ERK responses (Das *et al.*, 2009; Jun *et al.*, 2013). In contrast, we show here that in PDBu-stimulated Ramos B-cells (a condition in which SOS is not activated) that Ras activation is graded, whereas ERK

activation remains digital (Figure 6, C–E). How might this discrepancy be explained? One possibility is that there are key differences in Ras-ERK pathway components between the Ramos B-cells used in this study and the cells used in Das *et al.* (2009). Another possibility is that our work performed in living single cells may accentuate signaling responses that are masked in population level experiments performed previously (Das *et al.*, 2009; Jun *et al.*, 2013). However, it is important to note that we and Das *et al.* (2009) both examine phorbol ester-induced ppERK in Jurkat T-cells at the population level (Supplemental Figure S8B) and come to differing conclusions (bimodal vs. graded, respectively).

Future work that leverages the live cell biosensors used in this study to examine Ras-ERK signaling in single living primary lymphocytes will aid in resolving this discrepancy.

Feedback activation of SOS by RasGTP is the predominant mechanism invoked to explain the bimodal nature of activation of the Ras pathway effectors (e.g., ERK, CD69). However, positive feedback and amplification at the level of Ras activation is just one mechanism capable of generating bimodal responses. Signaling protein oligomerization and phase separation, for example, provide additional mechanisms for initiating nonlinear biochemical responses (Li, Banjade, Cheng, *et al.*, 2012). Indeed, recent studies highlight the ability of GRB2 and SOS to form phase-separated aggregates in activated T-cells (Huang *et al.*, 2016; Su *et al.*, 2016). Moreover, active Ras molecules have been shown to form homotypic nanoclusters capable of digitizing downstream ERK signaling in EGF stimulated baby hamster kidney cells (Tian *et al.*, 2007). It will be interesting to evaluate how each of these mechanisms contribute to the Ras pathway signaling dynamics we describe here.

We previously used a set of optogenetic tools to characterize the signal transmission between active Ras and downstream ERK in 3T3 fibroblast cells (Toettcher *et al.*, 2013). There we found near-linear transmission of Ras signals downstream to ERK nuclear localization. In contrast, our data here support a model in which an independent analogue-to-digital converter drives ERK activation once active Ras exceeds a threshold level. What mechanisms might explain this discrepancy? In *Xenopus*, positive feedback within the MAPK cascade mediates digital pathway activity, whereas in yeast, a zero-order ultrasensitivity in the disassociation of Fus3 (the yeast MAPK) from the scaffold protein Ste5 mediates switch-like responses (Ferrell and Machleder, 1998; Malleshaiah *et al.*, 2010). Pairing optogenetics with genomic and proteomic approaches will provide a framework for uncovering these differences in Ras pathway network architecture that underlies the differences in signaling responses between lymphocytes and fibroblasts (Toettcher *et al.*, 2013; Wilson *et al.*, 2017).

We have shown that analogue Ras signals give rise to digital ERK responses, suggesting that consecutive digital switches exist at the level of Ras and ERK activation during normal BCR signaling. Why organize the Ras-MAPK pathway in this manner? One possibility is that switch-like Ras responses serve to digitize activation of other Ras effectors (besides Raf), such as PI3K and PKCζ. As bimodal Ras responses bracket the switch point for ERK kinase activity (Figure 5, B and E), it is also possible that these sequential switches could confer robustness to MAPK activation. Last, lymphocytes are thought to integrate antigen signals in time during serial APC engagement (Zikherman and Au-Yeung, 2015). Hysteresis in Ras activity could act as a molecular memory of previous antigen exposure. Our work provides a foundation for investigating how these multiple sources of signal amplification enable B-cells to convert the magnitude, duration, and frequency of antigen exposure into appropriate cellular activation.

MATERIALS AND METHODS

Cell culture
Ramos cells were obtained from the American Type Culture Collection. Jurkat cells were a kind gift from A. Weiss (University of California, San Francisco [UCSF]). Both Jurkat and Ramos cells were maintained in 10G-RPMI (RPMI 1640 supplemented with L-glutamine and 25 mM HEPES [Mediatech] and containing 1% [vol/vol] GlutaMAX [Life Technologies] and 10% [vol/vol] fetal bovine serum [FBS; Life Technologies]). Cultures were maintained in a 37°C/5% CO_2 incubator at a density ranging from 0.2 to 1 million cells/ml. HEK-293T cells (used to generate lentivirus for transduction) were maintained in DMEM (Mediatech) supplemented with 10% (vol/vol) FBS (Life Technologies). Cells were imaged in imaging media (RPMI 1640 without phenol red supplemented with 25 mM HEPES, 1% L-glutamine, and 0.1% FBS).

Plasmids
All constructs were cloned into the pHR lentiviral backbone (kindly provided by R. D. Vale, UCSF) containing the spleen focus-forming virus promoter via standard Gibson assembly. Human cRaf/Raf1 cDNA was a gift from W. Loomis (University of California, San Diego). RBD[51-131] and RBD[51-220] coding sequences were amplified from this cDNA and subcloned into a GFP containing pHR vector to generate pHR-RBD-GFP and pHR-RBD[220]-GFP plasmids, respectively. The ERK[KTR] sequence was amplified from pLentiCMV-Puro-ERK[KTR]-Clover (Addgene # 59150) and subcloned into a pHR vector containing TagRFP-T to generate pHR- ERK[KTR]-TagRFP-T. Murine GRB2 cDNA (kindly provided by M. Davis, Stanford University) was amplified and subcloned into a pHR plasmid containing TagBFP to generate pHR-GRB2-BFP.

Cell line generation and stimulation
Cell lines were generated via lentiviral transduction. Lentivirus was produced by cotransfecting vectors encoding lentiviral packaging proteins (pMD2.G and p8.91) along with a pHR vector containing a gene of interest into Hek-293T cells plated in six-well plates (Thermo Fisher Scientific) grown to ~70% confluence. Transit-IT-293 (Mirus Bio) was used for all transfections. Viral supernatants were harvested 2 d posttransfection, filtered through a 0.45-μm syringe filter (Millex), and concentrated ~40-fold using a Lenti-X Concentrator (Takara Bio). Viral supernatants were either used immediately, stored at 4°C for up to 1 wk, or stored at –80°C for long-term storage. The 0.5 × 10^{6} Ramos cells resuspended in 250 μl 10G-RPMI were mixed at a 1:1 ratio with concentrated supernatant and incubated overnight. Following incubation, viral supernatants were removed by centrifugation, and transduced cells were cultured in 10G-RPMI for 1 wk to recover. Transgene-expressing cells were isolated by FACS. Clonal RBD[220]-eGFP/ERK[KTR]-Tag-RFP-T coexpressing cells were isolated by limiting dilution. IgM-deficient Ramos cells were isolated by iterative rounds of sorting Ramos cells negative for cell surface IgM expression (assayed by cell surface staining with APC-conjugated anti-IgM antibody, BioLegend #314509).

Cells were stimulated as indicated in the text and figure legends. The αIgM (BioLegend # 314502), PDBu (CST #12808S), and ConA (Sigma # C5275) were used at the indicated concentrations and were diluted in imaging media. The αMM (Sigma #M6882) was used at a final concentration of 100 mM and a fresh stock diluted fresh in imaging media for every experiment (to guard against contamination). PMA (Sigma #P1585), GÖ 6983 (Tocris # 2285), and BAY-61-3606 (Selleckchem #S7006) were used at the concentrations indicated in figure legends and were diluted in imaging media.

Microscopy and image analysis

Cells were plated in a well of a glass bottom 96-well glass plate (Corning). Wells were coated with 1 mg/ml poly-L-lysine (Sigma) for ~30 min and washed 3× with phosphate-buffered saline (PBS) prior to cell seeding (at a concentration of 0.5 million cells/ml). Images were acquired on a Nikon Eclipse Ti inverted microscope equipped with a Yokogawa CSU-X1 spinning disk confocal, a 60 × 1.4 Plan Fluor objective (Nikon), and a Prime95B cMOS camera (Photometics). Laser lines (405, 488, 561, and 640 nm [LMM5, Spectral Applied Research]) were used for excitation. CellProfiler (Broad Institute) and Fiji (National Institutes of Health) were used for cell segmentation and image analysis. Excel (Microsoft), Pandas (Wes McKinney, Ursa Labs), PRISM 7 (GraphPad), and Seaborn (Micahel Waskom, New York University) were used for data wrangling and visualization. For experiments in cells expressing ERK-KTR, nuclei were labeled with NucBlue (Thermo Fisher Scientific) per manufacturer instructions.

Raw microscopy images were background subtracted and corrected for stage drift prior to cell segmentation (to identify cells) and erosion (to remove peripheral pixels and identify the cytoplasm). Membrane intensity of signaling activity reporters (Ras, GRB2) was calculated by taking the inverse of the cytoplasmic intensity. Singe cell intensity traces were normalized by dividing traces by a cell's integrated mean fluorescence prior to stimulation.

The cytoplasmic-to-nuclear ratio of KTR channel intensity was used to quantify KTR activity. The fluorescence intensity of KTR reporter was quantified in the nucleus (identified by NucBlue signal) and the cytoplasm (identified by subtracting nuclear region of the cell from the cell mask). Owing to the scarcity of cytoplasmic pixels in Ramos cells, the consistency of cell masking from frame to frame was evaluated and adjusted manually for KTR quantitation. As nuclei occupy a large fraction of the cytoplasmic area in Ramos cells, for experiments in which both Ras reporter and KTR signal was measured, cells were imaged at both a coverslip proximal focal plane (to exclude the nucleus and improve Ras reporter quantitation; Supplemental Figure S1) and an equatorial focal plane (to include the nucleus and facilitate KTR quantitation).

All imaging experiments were performed at least two (and generally three) times. Dead cells were identified by eye and excluded from analysis.

Statistical analysis

Two-tailed Student's t tests were performed using PRISM 7 software (GraphPad). Tests with a p value < 0.05 were considered statistically significant. In figures, ns indicates not significant, whereas * p < 0.05, ** p < 0.01, and *** p < 0.001. Hartigans' dip test was performed in R (diptest package; Martin Maechler, ETH Zurich). Tests with a p value <0.05 indicate significant bimodality, whereas tests with p values > 0.05, but <0.1 indicated bimodality with marginal significance. The dip statistic (D) indicates the point in a population distribution in which the maximal difference between peaks in the distribution is achieved. For our purposes, it highlights a plausible separation between populations of cells responding to stimulation.

Western blots and FACS

For Western blot experiments, cell lines were serum-starved for 0.5–1 h in imaging media at a concentration of $0.5 × 10^6$ cells/ml. Following stimulation, cells were immediately transferred to ice, pelleted via centrifugation, and resuspended in 200 μl ice-cold lysis buffer (1% Triton X-100, 50 mM HEPES, pH 7.4, 150 mM NaCl, 1.5 mM $MgCl_2$, 1 mM egtazic acid, 100 mM NaF, 10 mM Na pyrophosphate, 1 mM Na_3VO_4, 10% glycerol, freshly supplemented with protease and phosphatase inhibitor tablets [Roche Applied Sciences]). Lysates were incubated on ice for 10 min and centrifuged at $15,000 × g$ for 10 min. Protein concentration was measured by BCA Assay (Thermo Fisher Scientific), after which samples were solubilized in 4× sample buffer (Bio-Rad Laboratories) and boiled at 100°C for 10 min. Samples were either immediately loaded onto gels for Western blot analysis or flash-frozen. Bolt 17-well precast 4–12% Bis-Tris Plus gels (Thermo Fisher Scientific) were run at 200 V for 25 min to resolve proteins. Proteins were transferred from gels to nitrocellulose membranes using a Trans-Blot semidry transfer apparatus (Bio-Rad) run at 20 V for 1 h. Membranes were blocked in Odyssey Blocking Buffer (LI-COR) for 1 h, exposed to primary antibodies diluted according to manufacturer instructions in Odyssey Blocking Buffer for 4°C overnight, washed in TBST, and incubated in IRDye (LI-COR) anti-rabbit and anti-mouse secondary antibodies for 30 min at room temperature. Following a final wash in TBST, membranes were imaged using a LI-COR imaging station. Anti-pTyrosine (CST #8954) and Anti pRasGRP3 (T133) (CST #3334) were used at 1:1000 dilutions.

Cell surface staining experiments (IgM, CD22) were performed in FACs buffer (PBS, 5% FBS, 1 mM EDTA, 0.1% NAN_3) for 30 min at 4°C. Cells were washed 3× in ice-cold FACs buffer, fixed at room temperature in Cytofix (BD Biosciences), washed three additional times in FACs buffer, and run immediately on a BD LSR II (BD Biosciences). For FACs staining of ppERK, cells were serum-starved as above in 96-well plates (Corning). A 2× stock of stimulus (IαGM, PDBu, etc.) was used to stimulate cells for the appropriate time. Cells were then fixed at room temperature with Cytofix (BD Biosciences), pelleted by centrifugation (500 × g for 5 min), and resuspended in ice-cold methanol to permeabilize cell membranes overnight. Cells were washed 3× in ice-cold FACS buffer and stained with anti-ppERK antibody (CST #4370) diluted 1:1000 in FACs buffer for 1 h at room temperature. Cells were washed 3× in FACs buffer and stained with 405 conjugated anti-rabbit secondary antibodies (Abcam #ab175672) for 30 min. Cells were washed three additional times in ice-cold FACS buffer and run immediately on BD LSR II (BD Biosciences). Analysis of flow cytometry data was performed in FlowJo.

REFERENCES

Boldface names denote co–first authors.

Anderson DJ, Durieux JK, Song K, Alvarado R, Jackson PK, Hatzivassiliou G, Ludlam MJC (2011). Live-cell microscopy reveals small molecule inhibitor effects on MAPK pathway dynamics. PLoS One, 6. doi: 10.1371/journal.pone.0022607.

Augsten M, Pusch R, Biskup C, Rennert K, Witting U, Beyer K, Blume A, Wetzker R, Friedrich K, Rubio I (2006). Live-cell imaging of endogenous Ras-GTP illustrates predominant Ras activation at the plasma membrane. EMBO Rep 7, 46–51.

Bondeva T, Balla A, Várnai P, Balla T (2002). Structural determinants of Ras-Raf interaction analyzed in live cells. Mol Biol Cell 13, 2323–2333.

Boykevisch S, Zhao C, Sondermann H, Phillippidou P, Halegoua S, Kuriyan J, Bar-Sagi D (2006). Regulation of Ras signaling dynamics by Sos-mediated positive feedback. Curr Biol 16, 2173–2179.

Chakraborty AK, Das J, Zikherman J, Yang M, Govern CC, Ho M, Weiss A, Roose J (2009). Molecular origin and functional consequences of digital signaling and hysteresis during ras activation in lymphocytes. Sci Signal 14, pt2.

Chiu VK, Bivona T, Hach A, Bernard Sajous J, Silletti J, Wiener H, Johnson RL II, Cox AD, Phillips MR (2002). Ras signalling on the endoplasmic reticulum and the Golgi. Nat Cell Biol 4, 343–350.

Christensen SM, Tu HL, Hun JE, Alvarez S, Triplet MG, Iwig JS, Yadav KK, Bar-Sagi D, Roose JP, Groves JT (2016). One-way membrane trafficking of SOS in receptor-triggered Ras activation. Nat Struct Mol Biol, 23, 838–846.

Das J, Ho M, Zikherman J, Govern C, Yang M, Weiss A, Chakraborty AK, Roose JP (2009). Digital signaling and hysteresis characterize Ras activation in lymphoid cells. Cell 136, 337–351.

Ferrell JE Jr, Ha SH (2014). Ultrasensitivity part III: cascades, bistable switches and oscillators. Trends Biochem Sci 39, 612–618.

Ferrell JE Jr, Machleder EM (1998). The biochecmical basis of an all-or-none cell fate switch in Xenopus oocytes. Science 280, 895-898.

Hartigan JA, Hartigan PM (1985). The dip test of unimodality. Ann Stat 13, 70–84.

Hibino K, Shibata T, Yanagida T, Yasushi S (2009). A RasGTP-induced conformational change in C-RAF is essential for accurate molecular recognition. Biophys J 97, 1277–1287.

Huang J, Brameshuber M, Zeng X, Xie J, Li QJ, Chien YH, Valitutti S, Davis MM (2013). A single peptide-major histocompatibility complex ligand triggers digital cytokine secretion in CD4+T cells. Immunity 39, 846–857.

Huang WYC, Yan Q, Lin W-C, Chung JK, Hansen SD, Christensen SM, Tu H-L, Kuriyan J, Groves JT (2016). Phosphotyrosine-mediated LAT assembly on membranes drives kinetic bifurcation in recruitment dynamics of the Ras activator SOS. Proc Natl Acad Sci USA 113, 8218–8223.

Iversen L, Tu HL, Lin WC, Christensen SM, Abel SM, Iwig J, Wu HJ, Gureasko K, Rhodes C, Petit RD, et al. (2014). Ras activation by SOS: allosteric regulation by altered fluctuation dynamics. Science 345, 50–54.

Iwig JS, Vercoulen Y, Das R, Barros T, Limnander A, Che Y, Peleton JG, Wemmer DE, Roose JP, Kuriyan J (2013). Structural analysis of autoinhibition in the Ras-specific exchange factor RasGRP1. eLife 2013, 1–28.

Jun JE, Yang M, Chen H, Chakraborty AK, Roose JP (2013). Activation of extracellular signal-regulated kinase but not of p38 mitogen-activated protein kinase pathways in lymphocytes requires allosteric activation of SOS. Mol Cell Biol 33, 2470–2484.

Li P, Banjade S, Cheng HC, Kim S, Chen B, Guo L, Liaguno M, Hollingsworth JV, King DS, Banani SF, et al. (2012). Phase transitions in the assembly of multivalent signaling proteins. Nature 483, 336–340.

Lorenzo PS, Behesti M, Petit GR, Stone JC, Blumberg PM (2000). The guanine nucleotide exchange factor RasGRP is a high-affinity target for diacylglycerol and phorbol esters. Mol Pharmacol 57, 840–846.

Malleshaiah MK, Shahrezaei V, Swain PS, Michnick SW (2010). The scaffold protein Ste5 directly controls a switch-like mating decision in yeast. Nature 465, 101–105.

Margarit SM, Sondermann H, Hall BE, Nagar B, Hoelz A, Pirruccello M, Bar-Sagi D, Kuriyan J (2003). Structural evidence for feedback activation by RasGTP of the Ras-specific nucleotide exchange factor SOS. Cell 112, 685–695.

Mochizuki N, Tamashita S, Kurokawa K, Ohba Y, Nagai T, Miyawaki A, Matsuda M (2001). Spatio-temporal images of growth-factor-induced activation of Ras and Rap1. Nature 411, 1065–1068.

Ogura Y, Wen FL, Sami MM, Shiabata T, Hayashi S (2018). A switch-like activation relay of EGFR-ERK signaling regulates a wave of cellular contractility for epithelial invagination. Dev Cell 46, 162–172.e5.

Oliveira AF, Yasuda R (2013). An improved Ras sensor for highly sensitive and quantitative FRET-FLIM imaging. PLoS One 8, 1–5.

Regot S, Hughey JJ, Bajar BT, Carrasco S, Covert MW (2014). High-sensitivity measurements of multiple kinase activities in live single cells. Cell 157, 1724–1734.

Rubio I, Grund S, Song SP, Biskup C, Bandemer S, Fricke M, Förster M, Graziani A, Witting U, Kliche S (2010). TCR-induced activation of Ras proceeds at the plasma membrane and requires palmitoylation of N-Ras. J Immunol 185, 3536–3543.

Shindo Y, Iwamoto K, Mouri K, Hibino K, Tomita M, Kosako H, Sako Y, Takahashi K (2016). Conversion of graded phosphorylation into switch-like nuclear translocation via autoregulatory mechanisms in ERK signaling. Nature 20, 10485.

Spencer SL, Sorger PK (2011). Measuring and modeling apoptosis in single cells. Cell 144, 926–939.

Su X, Ditlev JA, Hui E, Xing W, Banjade S, Okurt J, King DS, Taunton J, Rosen MK, Vale RD (2016). Phase separation of signaling molecules promotes T cell receptor signal transduction. Science 352, 595–599.

Takeda K, Shao D, Adler M, Charest PG, Loomis WF, Levine H, Groisman A, Rappel WJ, Flirtel RA (2012). Incoherent feedforward control governs adaptation of activated Ras in a eukaryotic chemotaxis pathway. Sci Signal 5, ra2.

Teixeira C, Stang SL, Zheng Y, Beswick NS, Stone JC (2003). Integration of DAG signaling systems mediated by PKC-dependent phosphorylation of RasGRP3. Blood 102, 1414–1420.

Thapar R, Williams JG, Campbell SL (2004). NMR characterization of full-length farnesylated and non-farnesylated H-Ras and its implications for Raf activation. J Mol Biol 343, 1391–1408.

Tian T, Harding A, Inder K, Plowman S, Parton RG, Hancock JF (2007). Plasma membrane nanoswitches generate high-fidelity Ras signal transduction. Nat Cell Biol 9, 905–914.

Toettcher JE, Weiner OD, Lim WA (2013). Using optogenetics to interrogate the dynamic control of signal transmission by the Ras/Erk module. Cell 155, 1422–1434.

Weiss A, Shields R, Newton M, Manger B, Imboden J (1987). Ligand-receptor interactions required for commitment to the activation of the interleukin 2 gene. J Immunol 138, 2169–2176.

Williams JG, Drugan JK, Yi G-S, Clark GJ, Der CJ, Campbell SL (2000). Elucidation of binding determinants and functional consequences of Ras/Raf-cysteine-rich domain interactions. J Biol Chem 275, 22172–22179.

Wilson MZ, Ravindran PT, Lim WA, Toettcher JE (2017). Tracing information flow from Erk to target gene induction reveals mechanisms of dynamic and combinatorial control. Mol Cell 67, 757–769.e5.

Zheng Y, Liu H, Coughlin J, Zheng J, Li L, Stone JC (2005). Phosphorylation of RasGRP3 on threonine 133 provides a mechanistic link between PKC and Ras signaling systems in B cells. Blood 105, 3648–3654.

Zikherman J, Au-Yeung B (2015). The role of T cell receptor signaling thresholds in guiding T cell fate decisions. Curr Opin Immunol 33, 43–48.